Electronic Supplementary Information

Computational analysis of the orientation persistence length of the polymer chain orientation

Falk Niefind, Andreas Neff, Stefan C. B. Mannsfeld, Axel Kahnt and Bernd Abel

Contents

1. Defining the chain orientation and the dichroism

The chain orientation, mentioned in Figure 1a) in the main paper, is defined as the in-plane direction of the molecular backbone of the polymer. For illustrative purposes, we have added arrows to indicate the chain orientation to Figure 1a) from the main paper here:

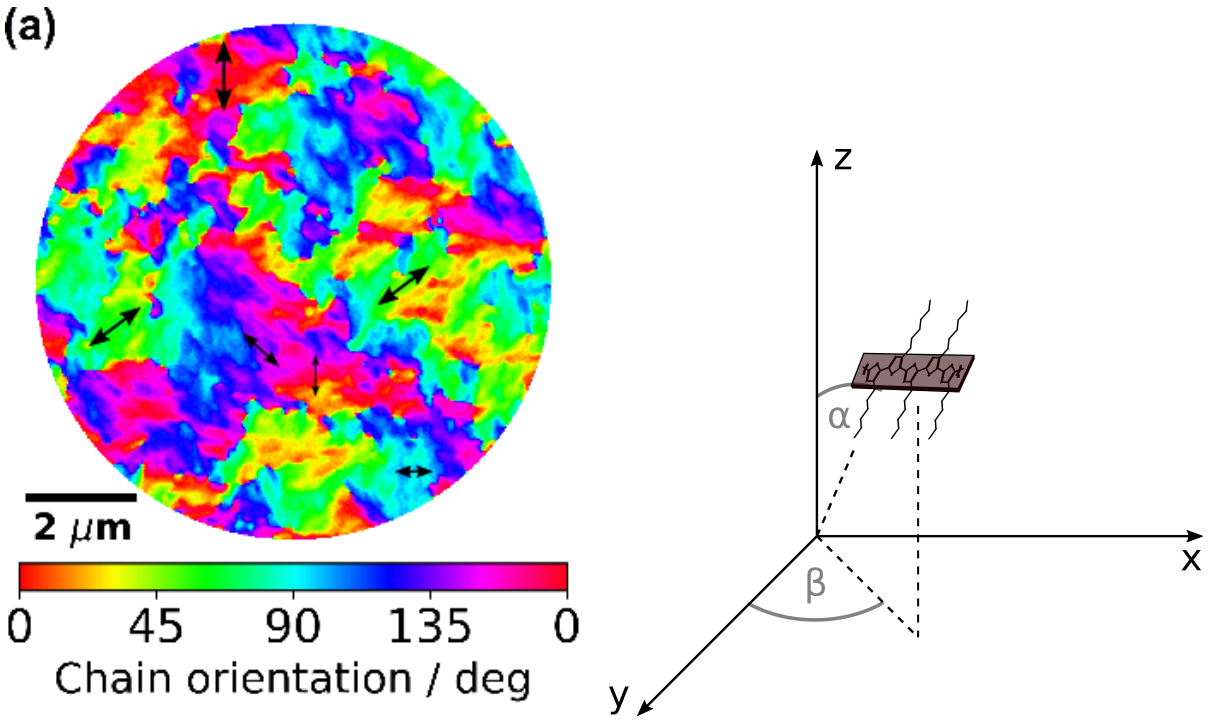

Figure S1: Left: Figure 1a) from the main paper with the addition of arrows indicating the polymer chain orientation in the different domains. Right: Illustration of the in-plane (β) and out-of-plane orientation α of polymer chains. The chemical structure of P3HT was taken as an example. The substrate is located in the x-y plane. Adapted from Watts et al [1].

For a deailed desciption of the dichroism please see the report by Neff et al.[2] In short, we obtain a stack of PEEM images with different laser polarisations. We then employ the formular

$$I_{\mathrm{el,P3HT}} = A \cdot cos^2\left(\alpha_{\mathrm{refl}} - \beta\right) + C \tag{1}$$

to every pixel in the image. Where A is the amplitude, C the offset, α_{refl} the polarization direction of the laser light and β the fit parameter, that also represents the chain orientation. The dichroism is then computed by

$$\rho = \frac{A}{2C + A}. \tag{2}$$

2. Finding the best parameters to describe the experimental results

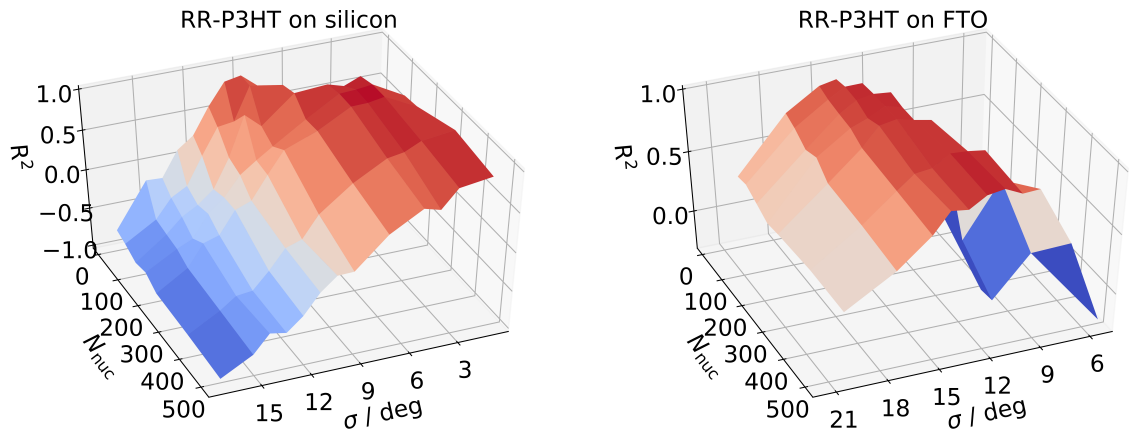

Figure S2: Plot of the R^2 values obtained from comparison between experimental and simulated OPL values depending on σ and N_{nuc}. While for the film on silicon a well-defined maximum around $\sigma \sim 3°$ and $N_{\text{nuc}} \sim 150$ was found (left part). For the film on FTO, R^2 is maximal for σ in the range of 11-14° depending on the number of crystallization centers (right part).

For the film on silicon, we observe a well-defined maximum for $\sigma \sim 3°$ and $N_{\text{nuc}} = 150$. In contrast, for the film on FTO we find a maximum of R^2 for σ in the range of 11-14°. For smaller values of N_{nuc} the maximum is located at larger σ. With increasing N_{nuc}, the maximum shifts to smaller values of σ while sustaining comparable values of R^2. This behavior can be understood in the way that both high values of σ and larger numbers of crystallization centers introduce disorder in the film. For some range of values, the effect of a larger number of crystallization centers can be accounted for by a smaller value of σ. In contrast, this does not work as well for the film on silicon, which exhibits very little disorder.

We note that the larger number of seeds, in case of the FTO sample, can originate from the higher amount of surface topography of the substrate, when compared to the sample spun onto the Si waver. We speculate that by increasing the film thickness , the effect of the surface topography should diminish.

3. Analyzing the results from the mathematical model

3.1. Reasoning for the hard border

The hard border was set at 5 μm to account for the limited field of view. In theory, the OPL could be bigger, as the starting pixels are selected from a circular area of 110 pixels in the center of the field of view. However, we expect this effect to vanish as we are averaging over 104 pixels and the traveled distance can also be shorter.

Another fact is that one can also travel diagonally, which would lead to an increased OPL. However, this effect is small, as the orientation maps gathered from the experiment exhibit a circular shape.

The effect that the OPL increases slightly due to the discrete size and rectangular shape is neglected here, as we are aiming to provide the simplest possible model that explains the experimentally observed trends.

3.2. Evaluating different simulation parameters

Constant μ: Within our model we assume, that the mean value of the Gaussian distribution does not change within one domain. Therefore, we modified the algorithm that generates the orientation maps in such a way, that each pixel is first assigned with a respective mean value μ_{pix}. Only after each pixel has received such a value, the function that draws from the Gaussian distribution is invoked for each pixel. This leads to a constant mean value μ within each domain. Only in the border regions the mean changes as the two domains are merging. In this case the algorithm determines the average value of μ_{pix} the same way as in the original algorithm. The only difference being, that the actual draw is only initiated, after each pixel in the whole map has a μ_{pix} assigned. In contrast, in the original algorithm, the draw from the Gaussian distribution is done before every pixel is set, resulting in a variation in μ_{pix} with respect to the neighboring pixels.

The results of the new algorithm are depicted in Figure S3. Comparing Figure S3 to Figure 4 in the main paper we can observe, that the modified maps exhibit significantly less disorder and that the domain size is significantly larger in Figure S3 at larger σ. This behavior was expected, as chance is only introduced at the last step of the map generation process and therefore cannot influence the orientation assigned to the neighboring pixels.

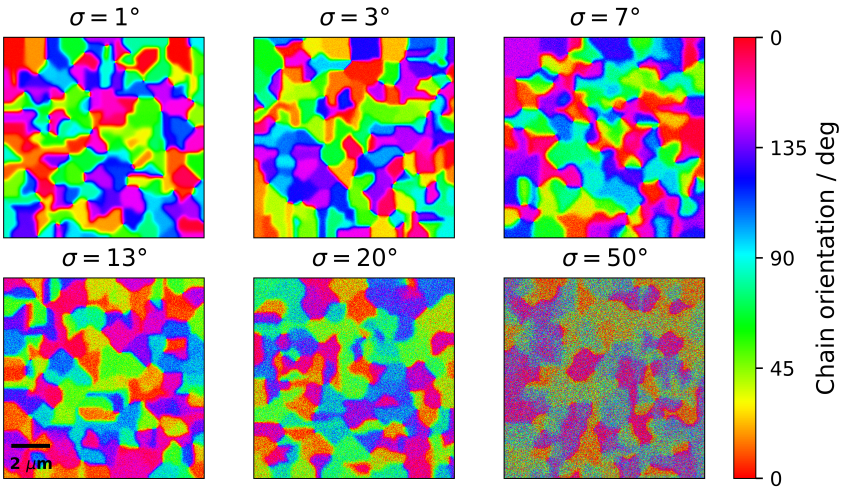

Figure S3: Simulated orientation maps for different standard deviations σ of the Gaussian distribution used for selecting orientation values. The mean of the Gaussian distribution μ is kept constant within one domain and does only change at the borders to a neighboring domain. The number of crystallization centers has been set to $N_{\text{nuc}} = 150$ for all images.

The results from the Monte Carlo algorithm are shown in Figure S4. Comparing Figure S4 to Figure 6 we can directly observe the result of the reduced disorder in the newly generated maps, leading to consistently higher OPLs. In addition, we can observe the cusps first encountered in the model also in the results from the Monte Carlo algorithm. They are especially pronounced at low σ and low N_{nuc}, which leads to the conclusion, that they are a product of the domain boundaries. With increasing σ and N_{nuc} the cusps vanish, as the border region gets less well defined due to the additional disorder. The OPL curves now depict a shape closer to the ones in Figure 6.

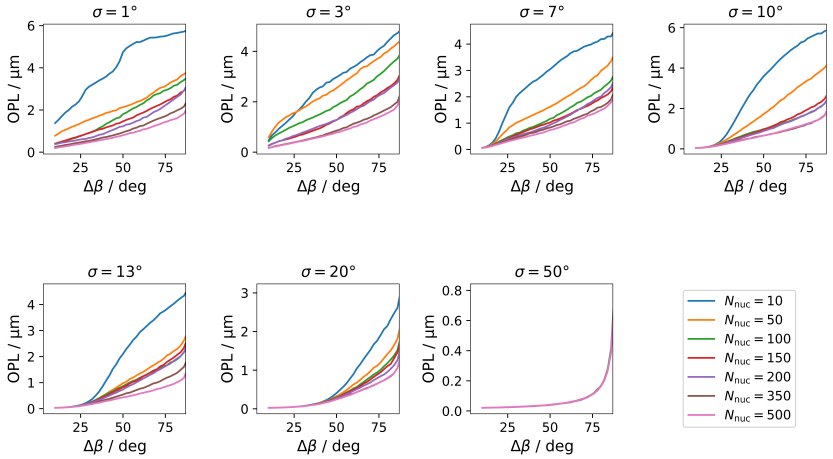

Figure S4: Dependence of the orientation persistence length on $\Delta\beta$ for the simulated orientation maps with a constant μ within the domains. We note, that in the data used for these plots, a significant amount of outliers is present for almost every curve, except the ones at $\sigma = 50°$ or for the ones with high N_{nuc}.

Hard borders: To further investigate the effect of border regions on the OPL we have crated orientation maps that only exhibit hard borders. They are displayed in Figure S5. To generate these maps, the original algorithm was modified in a way that pixels that have been assigned an orientation are not being overwritten in one of the next cycles.

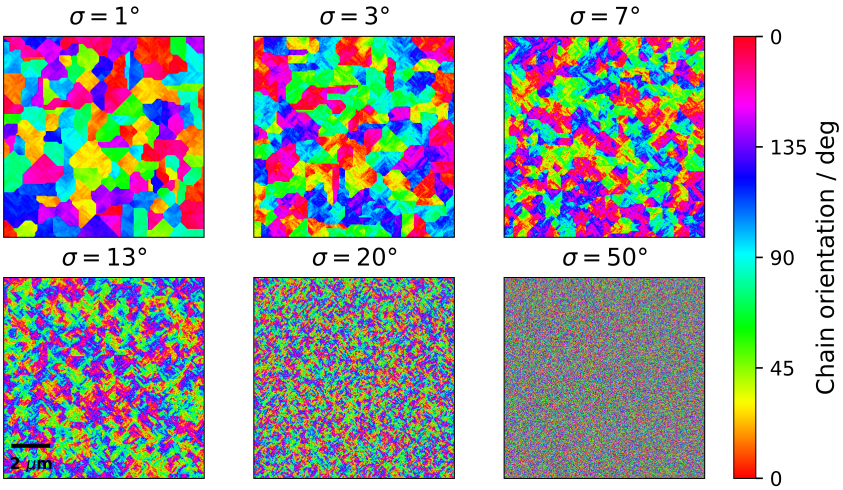

Figure S5: Simulated orientation maps for different standard deviations σ of the Gaussian distribution used for selecting orientation values. The hard borders were introduced by keeping the orientation of pixels that have been assigned through all the cycles of the algorithm. The number of crystallization centers has been set to $N_{\text{nuc}} = 150$ for all images.

Comparing Figure S5 to Figure 4 (paper main text) we can directly observe, that hard borders were successfully introduced. The resulting OPLs are depicted in Figure S6. Analyzing the results in Figure S6 we can, again, observe an increased overall OPL compared to the results from the original algorithm (cf. Figure 6). Once more, we attribute this to the decreased disorder in the newly generated maps. In the case of hard borders, the domains themselves are larger, as a smaller portion of the map is made up by border regions. The larger domains then lead to an increase in the OPL. However, when we compare the results of the maps with the constant μ (Figure S4) with the ones with the hard borders (Figure S6) we observe that the results from the maps with hard borders do not exhibit the distinctive cusps. Instead, especially for $\sigma = 1°$ or $\sigma = 3°$ we can observe the linear behavior at low values of $\Delta\beta$ that was previously seen in the results of the experimental results and the original simulated maps (cf. Figure 2 and Figure 5). Consequently, we conclude that the assumption of hard borders alone does not significantly contribute to the cusps and nonlinear behavior present in the results from our mathematical model.

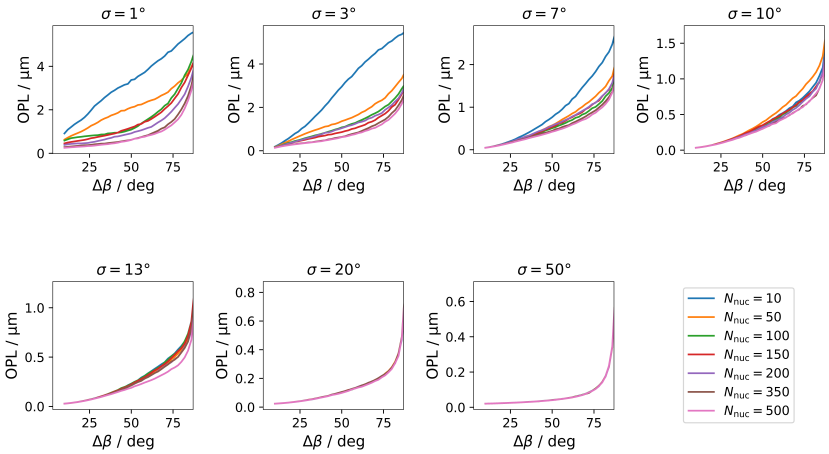

Figure S6: Dependence of the orientation persistence length on $\Delta\beta$ for the simulated orientation maps. We note, that in the data used for these plots, a significant amount of outliers is present for almost every curve at low σ.

4. Chemical structure of RR-P3HT

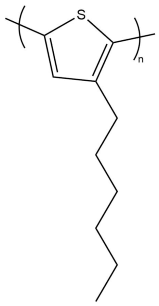

Figure S7: Chemical structure of RR-P3HT.

References

[1] B. Watts, T. Schuettfort, C. R. McNeill, *Advanced Functional Materials* **2011**, *21*, 1122–1131.

[2] A. Neff, F. Niefind, B. Abel, S. C. B. Mannsfeld, K. R. Siefermann, *Advanced Materials* **2017**, 1701012.